OPEN

Correspondence and
requests for materials
should be addressed to
B.-Y.C. (caoby@
tsinghua.edu.cn)

Anomalous orientations of a rigid carbon nanotube in a sheared fluid

Ruo-Yu Dong & Bing-Yang Cao

Key Laboratory for Thermal Science and Power Engineering of Ministry of Education, Department of Engineering Mechanics, Tsinghua University, Beijing 100084, P. R. China.

The nanoparticle orientation in fluid systems can be correlated with the rotational diffusion and is widely used to tune the physical properties of functional materials. In the current work, the controllability of the orientation of a single rigid carbon nanotube in a fluid is investigated by imposing a linear shear flow. Molecular dynamics simulations reveal three forms of anomalous behavior: (i) "Aligned orientation" when the nanotube oscillates around a particular direction which is close to the flow direction at a small angle of about 10° in the velocity-gradient plane; (ii) "Interrupted orientation" when the oscillation is interrupted by a 360° rotation now and then; (iii) "Random orientation" when 360° rotations dominate with the rotational direction coinciding with the local fluid flow direction. The orientation order is a function of the Peclet number (Pe). The results show that the correlation between Pe and the orientation order from the two-dimensional model does not apply to the three-dimensional cases, perhaps due to some anomalous behavior and cross-section effects. This work provides clear pictures of the nanoparticle movement that can be used to guide particle manipulation techniques.

Scientists are devoting more and more efforts to understanding the dynamics of active nanocomponents in soft matter systems for nonequilibrium conditions. Single-particle tracking experiments[1–4] have enabled real-time monitoring and have provided detailed information about the particle diffusion and directed motion. The rotary Brownian-type motion of a non-spherical nanoparticle, such as a carbon nanotube (CNT), which has been referred to as rotational diffusion in contrast to translational diffusion, has drawn considerable attention recently[5–10]. An external force field provides a confining potential which restricts the random nano-particle rotation[11,12]. The current study analyzes the combined effect of an applied moment and the Brownian torque that drives a single CNT to fall into some intriguing patterns, one of which is the orientation type. Orientation control of an elongated particle can benefit the *in vivo* particle transport[13] or biosensor designs[14]. The present study focuses on nanoparticles in large systems with this analysis of single particle orientation transferable to alignments of particles in dilute solutions where inter-particle interactions are not significant. CNT based nanocomposites and nanofluids have many useful features, with enhanced mechanical[15,16], electrical[17,18], optical[19] and thermal properties[20]. However, in nanofluids[21,22], the nanotubes arrange themselves randomly, which limits further improvements of the thermal conductivity of such nanofluids. The CNT's anisotropy suggests that an aligned distribution may further enhance the physical properties which will facilitate the processing and designing of advanced nanocomposites and related materials[23,24].

For carbon nanotube suspensions, the general constraint for the dilute regime where a study can focus on a single particle is $cL^3 \leq 1$, where c is the number density and L is the mean length of the nanotubes[25]. Furthermore, treating the CNT as a rigid rod-shaped object allows direct comparisons with classical theories. Jeffrey in 1922[26] gave a theoretical treatment of a rigid ellipsoid in a sheared viscous fluid which showed that, in the absence of Brownian motion, the ellipsoid would rotate indefinitely in a single parameter family of closed orbits, known as Jeffery orbits. A series of studies have discussed the Jeffery orbits[27–29] and the nontrivial effects of the very weak rotary Brownian motion on the rheological properties of suspensions[30] or single particle movements[31]. Molecular dynamics (MD) studies[32] have further confirmed Jeffery's theory by studying the motion of a low aspect ratio CNT in simple shear argon. This study showed that Brownian motion does account for the slightly different rotational time periods compared with the theory. Tannous[33] used a different method to derive the two dimensional (on the velocity-gradient plane) probability density functions from Langevin simulations for rigid solid objects. Tannous observed a preferred oriented distribution of rigid solid objects around the flow direction and the orientation order could be expressed as function of the Peclet number ($Pe = \dot{\gamma}/D_r$, where $\dot{\gamma}$ is the shear rate and D_r is the rotational diffusion coefficient). This conclusion was confirmed for liquid flows inside a planar channel geometry[33].
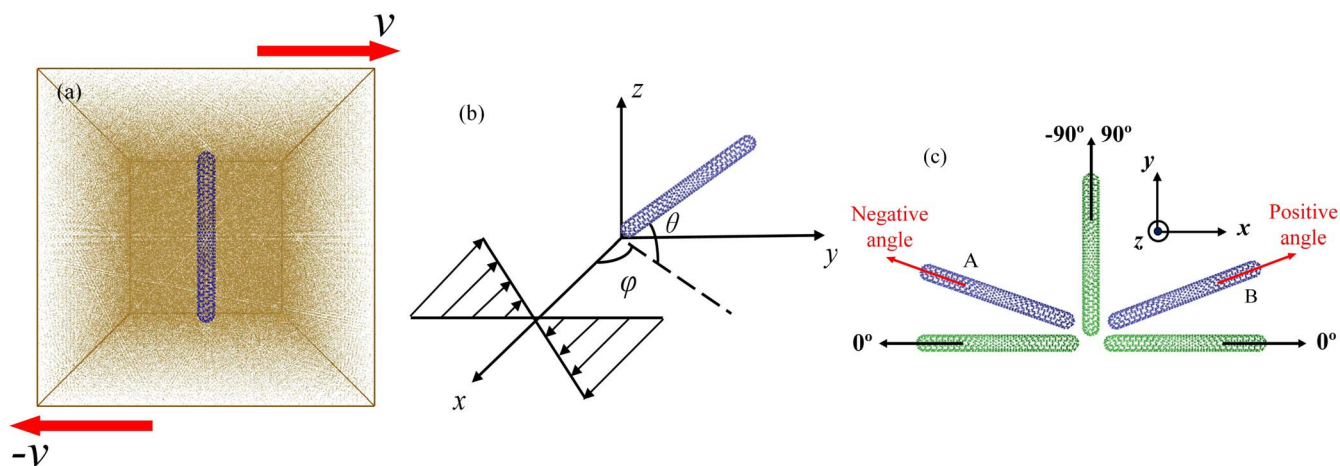
Figure 1 | (a) Schematic diagrams of the initial configuration of the simulation system and (b) definition of the orthogonal coordinates, x, y, z, longitudinal angle, φ, and latitudinal angle, θ, in the simple linear shear flow; (c) The angle range of the longitudinal angle, φ, in the x-y plane. The flow is along the x direction, while y is the gradient direction.

The studies in the literature still do not clarify under what circumstances a rigid solid object or a CNT would exhibit periodic rotations or would locate along an oriented direction[32,33]. This lack of understanding is the result of two problems. One is the lack of a clear physical view of the three-dimensional (3D) movement of the object, which cannot be obtained from two-dimensional theoretical treatments, while the other is due to insufficient observations and analyses of how different physical attributes affect the orientation. Actually, there is still uncertainty about whether the definition of Pe still applies to 3D rotary motion of an object. This work addresses these issues by investigating the orientation of a single rigid nanotube in a fluid undergoing a simple linear shear flow with the focus on the 3D orientation and the quantitative influence of various factors. This study uses a low aspect ratio CNT which can be treated as a rigid body to allow direct comparisons with theoretical results. The results with this simplified model can also be compared to experimental results with very large aspect ratio CNTs to analyze the effect of the rotational diffusion coefficient[1,5]. Molecular dynamics simulations are used for their simplicity in modeling the atom-atom interactions, the direct monitoring of the nanotube's Brownian motion and the ability to provide vivid pictures of how the nanotube actually moves. Unlike existing works, this study investigates the nontrivial coupling between the rotation, the orientation and the random Brownian motion of a nanoparticle, which results in various types of motion not observed in earlier studies.

Results

The MD simulation system was set up using orthogonal Cartesian coordinates, x, y, z, with longitudinal and latitudinal angles φ and θ

defined as in Figures 1(a), (b). The superimposed simple linear shear flow is illustrated in Figure 1(b) and given by Eq. (1),

$$v_x = \dot{\gamma} y, \ v_y = v_z = 0, \tag{1}$$

where $\dot{\gamma}$ stands for the shear rate. The carbon nanotube is surrounded by fluid argon and its long axis is initially parallel to the y direction. (In Supporting Information, the initial configuration is changed and no influences on the results can be observed: Figure S1 and Table S1) Although the simulations were performed in a 3D frame, the discussion mostly focuses on the x-y plane, which means that the directional angle is actually the longitudinal angle φ. Considering the fore-aft symmetry of the capped nanotube, the angle range is defined as shown in Figure 1(c). When the nanotube is parallel to the flow direction x, φ is equal to 0°. In the velocity gradient direction, φ may have a discontinuous jump from +90° to −90° and is negative for nanotube "A" and positive for nanotube "B" as shown in Figure 1(c). The base case is defined here with various factors then changed individually to examine their influences. The capped nanotube had the armchair (5, 5) configuration with a base case diameter, d, of 0.7 nm and length, L, of 6.8 nm. The density, ρ, of the argon was 1763 kg/m³ and the temperature, T, was 300 K, which corresponds to a supercritical state. The simulation domain had a size of $L_x \times L_y \times L_z = 10.6 \times 10.6 \times 10.6$ nm³. The shear rate was equal to 2×10^{10} s⁻¹ for the nonequilibrium simulations.

The orientation type of the nanotube will be affected by the properties of the nanotube, the fluid and the shear rate. To simplify the discussion, the length, L, of the nanotube is changed first to study the motion with the other factors held constant at the values in the base
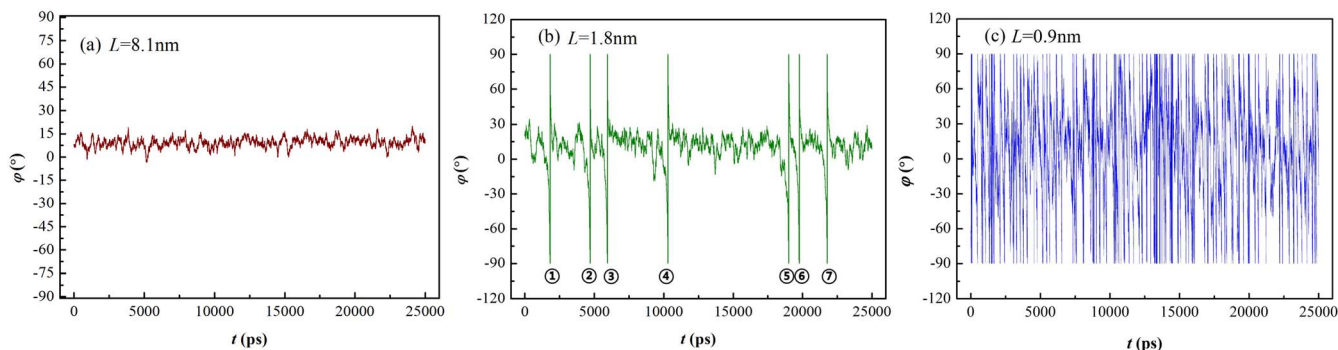
Figure 2 | Time-varying instantaneous angle φ for (a) $L = 8.1$ nm; (b) $L = 1.8$ nm; (c) $L = 0.9$ nm. Here, L denotes the length of the nanotube.
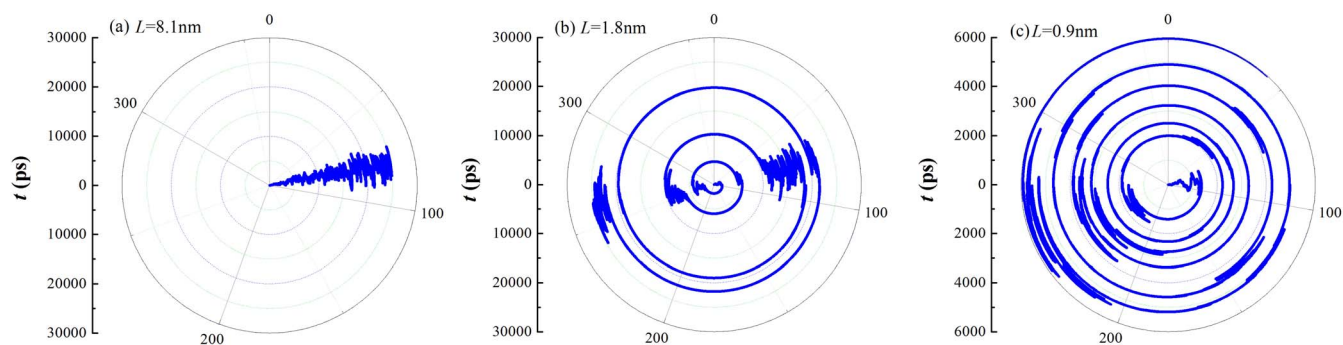
Figure 3 | Time-varying instantaneous angle φ with a range of 0° to 360° plotted in polar coordinates for (a) L = 8.1 nm; (b) L = 1.8 nm; (c) L = 0.9 nm. Here, L denotes the length of the nanotube. Here, the angle range is 0° to 360° to display a full circle of rotation, different from the definition in Figure 1(c). 0° means that the nanotube is parallel to the y direction.

case. Three types of motion appeared for the time-varying instantaneous angle, φ, as shown in Figures 2(a)–(c). Firstly, for L equal to 8.1 nm, the nanotube oscillates around a particular angle, approximately +10° from the flow direction (Figure 2(a)). Secondly, for L equal to 1.8 nm, most of the time, the nanotube still has a preferred orientation angle of around +10° with several circular rotations mixed into the oscillations now and then (Figure 2(b)). Finally, the nanotube with the smallest length rotated continuously all the time with no fixed angle (Figure 2(c)). As nanotube becomes shorter, the orientation of the nanotube becomes less ordered and the nanotube's orientation type can be classified into three forms as "aligned orientation", "interrupted orientation" and "random orientation". This anomalous behavior is interesting since there are no existing theories to predict this behavior, especially for the unusual interrupted orientation. The aligned orientation state is of particular interest due to its relevance to particle alignment. These observations can be better understood by plotting the instantaneous angles for the three forms in polar coordinates as in Figures 3(a)–(c). Now, the angle range is 0° to 360° to display a full circle of rotation. (Here, 0° means that the nanotube is parallel to the y direction which differs from the angle definition in Fig. 1(c) which applies to the rest of the manuscript.) The 360° rotations of the nanotube are always clockwise as seen in Figures 3(b)–(c), as was observed earlier[28,29]. This rotational direction can be anticipated for the superimposed linear shear given by Eq. (1) which creates a local clockwise vorticity while the viscous drag by the surrounding fluid induces a torque on the nanotube. In addition, no clear boundary exists between the interrupted and random orientations. The transition from the interrupted state to the random orientation state occurs when the nanotube's rotations dominate over the oscillations. Actually, these observations suggest that the occurrences of the orientation types are not always consistent and the complex combinations of mixed orientation and rotation types cannot be predicted theoretically[33].

The underlying mechanisms for these three types of orientation were further investigated by examining the nanotube's three dimensional movements as shown in Figures 4 and 5. Figures 4(a)–(c) show the projection of the time-varying ratio of the nanotube's length on the x-y plane while Figures 5(a)–(c) show the time-varying angular velocity, ω_z. At all times, the projection of the ratio is close to unity for the longest nanotube whose orientation type is aligned orientation (Figure 4(a)). This means that the nanotube is almost in the x-y plane with a very small latitude angle θ. For the random orientation case with L = 0.9 nm, the projection of the ratio varies greatly between 0 and 1 (Figure 4(c)). Thus, a nanotube that rotates out of the x-y plane with a larger angle θ, will be more likely to experience a 360° rotation away from the preferred orientation angle. As the latitudinal angle, θ, becomes larger, the nanotube rotates faster around the z axis. ω_z is approximately ±0.06 rad/ps for L = 8.1 nm (Figure 5(a)) and ±0.6 rad/ps for L = 0.9 nm (Figure 5(c)). Moreover, for the random orientation type, the time period for angle φ is approximately 834 ps. For an object rotating around Jeffery orbits with negligible Brownian effect[34], the time period is about 4490 ps as estimated from $T = \frac{2\pi}{\dot{\gamma}}\left(r_e + \frac{1}{r_e}\right)$ where $\dot{\gamma}$ is the shear rate and $r_e = 1.24\frac{L}{d}\sqrt{\ln\frac{L}{d}}$ is the equivalent aspect ratio[32]. Thus, these results indicate faster rotations for our simulations, which is reasonable considering the small friction imposed on the nanotube from the surrounding argon in the supercritical state. The interrupted orientation type is like a combination of the other two types. Specifically, seven rotations can be differentiated from the dominate oscillations (Figure 2(b)) with a marked decrease in projection of the ratio (Figure 4(b)) and a sudden distinct increase in the absolute value of ω_z as shown in Figure 5(b) with only one exception (No.④). As the projection ratio is equal to cosθ, the latitudinal angle
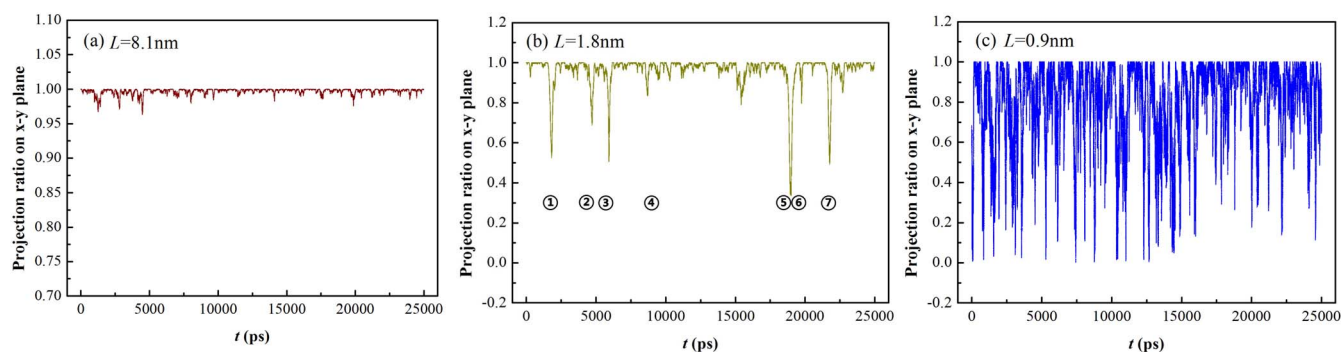
Figure 4 | Time-varying projection of the ratio of the nanotube's length on the x-y plane for (a) L = 8.1 nm; (b) L = 1.8 nm; (c) L = 0.9 nm. Here, L denotes the length of the nanotube.
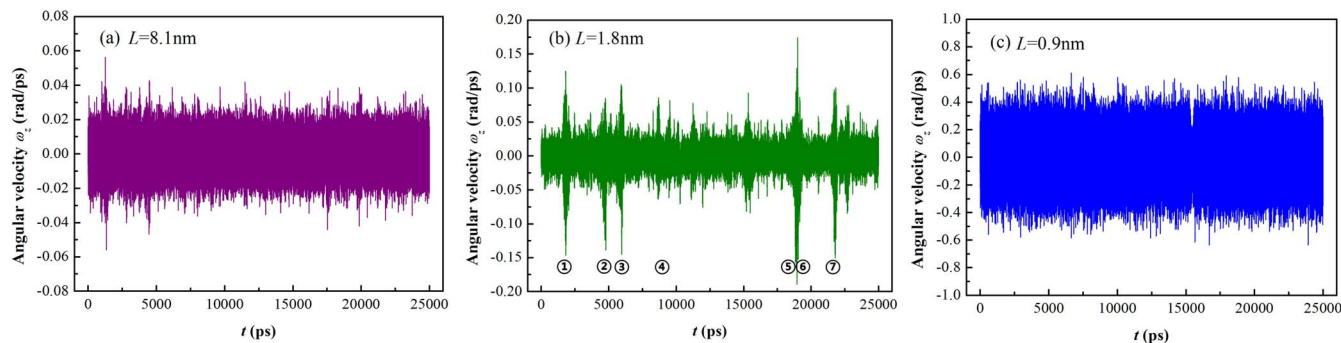
Figure 5 | Time-varying angular velocity, ω_z, for (a) $L = 8.1$ nm; (b) $L = 1.8$ nm; (c) $L = 0.9$ nm. Here, L denotes the length of the nanotube.

($0° \sim 90°$) is generally less than $40°$ (the ratio is larger than 0.8) for the oscillations and well above $40°$ when the rotations occur for these three cases. Thus, to have a good orientation, the nanotube should be confined to the x-y plane with a relatively small latitudinal angle. Otherwise, the $360°$ rotation is more likely to develop with a larger ω_z than during the oscillations.

The orientation variations upon changing the diameter, d, of the nanotube or the density, ρ, or temperature, T, of the argon are quite similar to that of changing L, with the results presented in the Supporting Information (Figures S2–S7). The qualitative trend is that increasing d or T, or decreasing ρ relative to the base case will cause the nanotube orientation type to shift from aligned to interrupted and then to the random orientation type. The corresponding 3D variations of the rotational direction, projection ratio and angular velocity are all quite similar. In addition, the nonequilibrium system approaches equilibrium as the shear rate decreases. At high shear, occasional oscillations around a particular angle can still be distinguished and the $360°$ rotation is always clockwise for the random orientation type (Figure 3(c)). However, for very low shear, the rotation is random and unpredictable (Figure 6). This phenomenon arises due to the increasing relative strength of the random Brownian couples relative to the mechanical torque due to the shear flow near equilibrium.

The Peclet number,

$$Pe = \dot{\gamma}/D_r, \qquad (2)$$

in which $\dot{\gamma}$ is the shear rate and D_r is the rotational diffusion coefficient, indicates the relative strength of the hydrodynamic interactions and Brownian forces and is, thus, a crucial parameter indicating the orientation order. To exhibit the results in terms of Pe, the rotational diffusion coefficient, D_r, must first be defined. Cao and Dong[35] calculated this diffusivity using equilibrium and nonequilibrium molecular dynamics methods. A detailed discussion of how to calculate D_r is presented in the Supporting Information (Figure S8 and Table S2). Pe can then be obtained from Eq. 2 for the simulation cases. The angle probability density distributions, $P(\varphi)$, has isolated peaks for the two different lengths in Figure 7 indicating that the nanotube shows preferred orientations around these particular angles. Higher peaks and narrower distribution ranges result in a more ordered orientation type for larger Pe. The higher peak appears for the larger Pe and the probabilities for angles away from this peak are nearly zero. For smaller Pe, the probabilities are almost the same over the entire angle range, indicating no preferred orientation angle. The present MD results do not agree well with the results of Tannous[33] shown in Figure 7. Although $P_{MD}(\varphi_{max}) = 0.629$ and $P_{[33]}(\varphi_{max}) = 0.608$ are quite close for $Pe = 4.36$, the large difference between $P_{MD}(\varphi_{max}) = 2.93$ and $P_{[33]}(\varphi_{max}) = 1.33$ for $Pe = 49.3$ should be noticed.
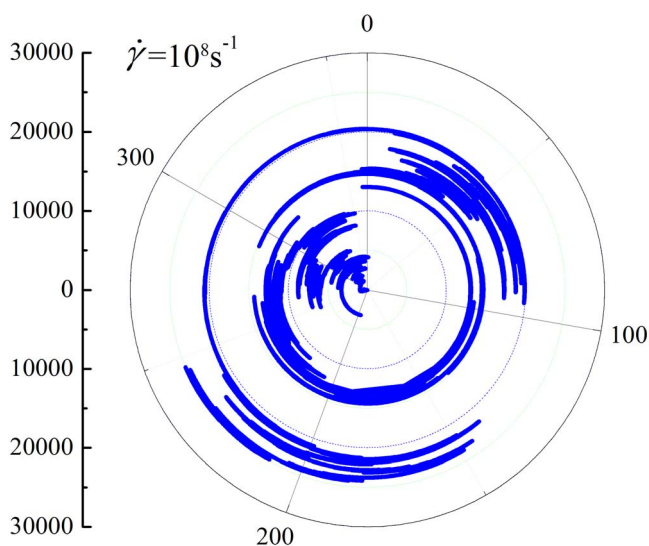
Figure 6 | Time-varying instantaneous angle φ with a range of $0°$ to $360°$ plotted in polar coordinates for shear rate $\dot{\gamma} = 1 \times 10^8$ s^{-1}.
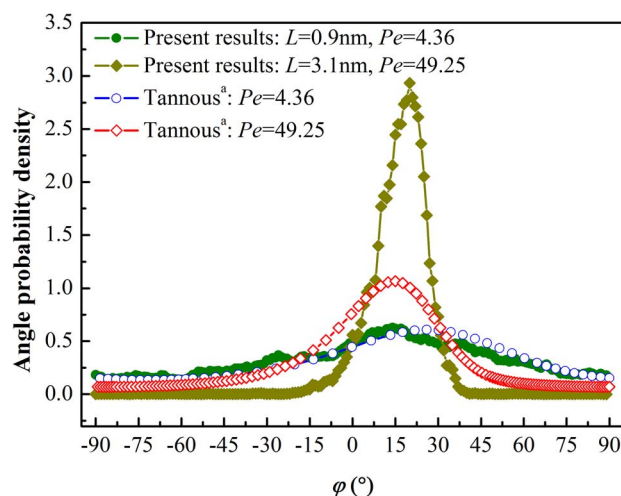
Figure 7 | Angle probability density distributions for two different nanotube lengths of 0.9 nm and 3.1 nm compared with theoretical results[33].
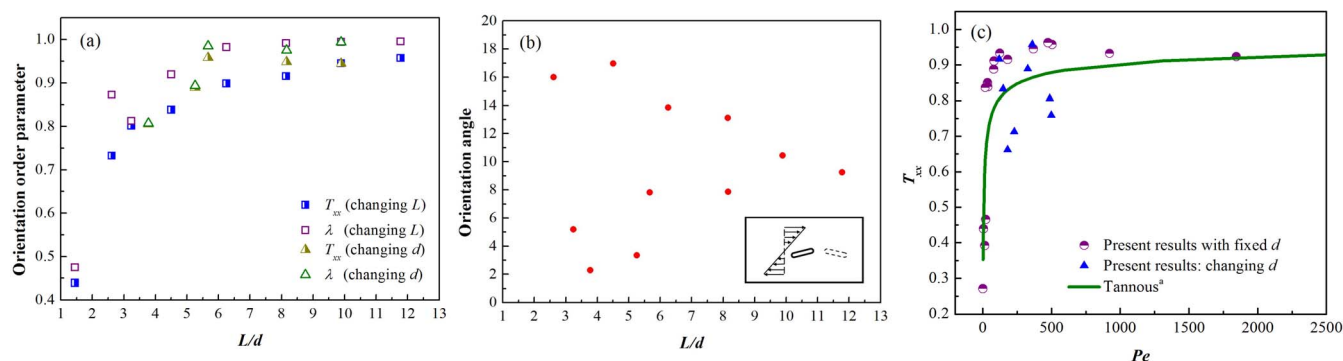
Figure 8 | (a) Dependence of the orientation order parameters T_{xx} and λ on the aspect ratio. The cases with different lengths, L, or diameter, d, are identified by different symbols; (b) Dependence of the orientation angle, φ, on the aspect ratio. The inset is a sketch of the nanotube placement to show that the nanotube has a positive angle with respect to the flow direction, as represented by the solid outline rather than the dotted outline; (c) Dependence of the orientation order parameters, T_{xx} on the Peclet number compared with theoretical results[33]. The cases of changes in the other factors with a fixed diameter are differentiated from the cases with different diameter with the other factors fixed by different symbols.

The nanotube orientation type can be further defined by the order tensor[36,37]:

$$T_{ij} = \frac{3}{2N} \sum_{n=1}^{N} \left[l_i^{(n)} l_j^{(n)} - \frac{1}{3} \delta_{ij} \right], \qquad (3)$$

where N is the total number of nanotubes and $\vec{l}^{(n)}$ is the unit axial direction vector. The subscripts i and j are selected between x and y since the orientation is only considered in the x-y plane. Thus, $\mathbf{T}$ is a 2 $\times$ 2 symmetric matrix. If the diagonal element $T_{ii} = 0.25$, the time-varying angles exhibit a completely random distribution. If $T_{ii} = 1$, the nanotube is perfectly oriented along the i axis. The largest eigenvalue of $\mathbf{T}$, symbolized as λ, is actually the orientation order along the most preferred angle, i.e. orientation angle φ_o, which is the corresponding eigenvector. The orientation order parameters, T_{xx}, and the largest eigenvalue λ of $\mathbf{T}$ were calculated for various aspect ratios (Figure 8(a)). The armchair configuration of (5, 5) to (12, 12) corresponding to a diameter change of 0.7 nm to 1.7 nm was used with the length varied from 0.9 nm to 8.1 nm. In all cases, λ is larger than T_{xx}, indicating that the preferred direction is not parallel to the x axis. Both of these parameters become closer to unity as the aspect ratio increases. In Figure 8(b), the orientation angles show no clear dependence on the aspect ratio, with all these angles in the interval of $(+2°, +18°)$, approximately consistent with Tannous[33]. Positive orientation angle mean that the nanotube is more likely in the state shown in the solid sketch in the inset of Figure 8(b) rather than the state shown by the dotted outline. Detailed results for the orientation order parameter and orientation angle are shown in the Supporting Information (Figure S9) for various densities, temperatures and fluid shear rates. The results show that with increasing fluid density, decreasing temperature, or increasing shear rate, the nanotube tends to become more oriented along a specified direction. The results also show that the orientation angle has a very slight dependence on these factors and is about $+10°$ relative to the flow direction. When λ is larger than about 0.95, the orientation type has the aligned orientation; when $0.6 < \lambda < 0.95$, the orientation type has the interrupted orientation; and when λ is less than 0.6, the orientation type is the random orientation.

The orientation order parameter, T_{xx}, was then calculated for various Pe for a large number of cases with the results for different nanotube diameters indicated by different symbols in Figure 8(c). One of the main conclusions in Tannous[33] was that a positive correlation exists between Pe and the orientation order parameter, T_{xx}. As can be seen, the MD results in Figure 8(c) clearly differ from Tannous's work with no positive correlation between T_{xx} and Pe. In particular, the diameter changes produce opposing trends. In

Figure 8(c), d is varied from 0.7 nm to 1.7 nm for two nanotube lengths of 4.3 nm and 6.8 nm. The diameter increase leads to a larger D_r as shown in Table S1 (Supporting Information) and a smaller orientation order as shown in Figure 8(a). This phenomenon may challenge whether the expression for Pe or its relationship with the orientation order established in Tannous[33] are valid.

Thus, in the same shear flow field, a more easily rotating nanotube with a larger D_r will not necessarily lead to a less ordered time-varying orientation with significant differences between the orientation states and the theoretical treatment in Tannous[33]. In fact, the 2D study by Tannous showed that the rigid solid object motion and the object's cross-sectional area are both negligible in the plane of the flow. As the nanotube is free to rotate in the 3D frame in the present study, so its movements may become quite complicated, as shown by the three anomalous orientation types discussed here. The additional effect due to the cross section may also be responsible for the differences from the theory, particularly as evidenced by the differences in the results as the diameter changes.

Discussion

To conclude, this study reveals anomalous orientation variations of a rigid carbon nanotube in a sheared fluid in molecular dynamics simulations. First, the orientation variations can be classified into three forms as the "aligned orientation", "interrupted orientation" and "random orientation", corresponding to the decreasing orientation order in each type. The relatively small projection of the nanotube length ratio onto the x-y plane means that the 360° rotation can more easily occur with a relatively larger angular velocity, ω_z, which will interrupt the oriented state even leading to the state of no orientation at all. Second, the nanotube has a preferred time-varying directional angle, i.e. a longitudinal angle, φ, of around $+10°$ from the flow direction. The time-varying orientation type is found to be affected by the length and diameter of the nanotube, as well as the density, temperature and shear rate of the fluid. Third, the Peclet number serves as an important scaling parameter for processing the results. The results show that the Peclet number does not positively correlate with the orientation order, especially as reflected by the results showing that the diameter increase does not reduce the order parameter. This breakdown may arise from the non-trivial cross sectional effect of the diameter and the nanotube's complex 3D rotational movements during the three types of motion. The nanoparticle rotational patterns could potentially be exploited to control the nanoparticle movement in bio-transport processes, the fabrication of materials with exceptional properties and other applications. We believe this work will benefit the study of dilute CNT suspensions and can be extended to other nanoparticle suspensions focusing

mainly on analysis of single particle motion. The CNT is assumed to be rigid as in many experimental investigations to allow direct comparisons with existing theories of rotational diffusion. Although the current results cannot be directly applied to concentrated suspensions, these results will serve as a useful point of reference for theoretical formalisms and experiments with concentrated suspensions that must incorporate the correct physics that holds in this limit. The anomalous behavior observed here encourages us to devote more efforts into modifying and developing theories to describe these behavior types, which will in turn serve as the foundation for more up-to-date design and analysis techniques.

Methods

The rodlike CNT nanotube molecule is capped at both ends to prevent argon atoms from entering the nanotube. The MD package LAMMPS was used for the calculations[38]. The forces between the argon atoms and between the argon and carbon atoms were calculated based on the Lennard-Jones (LJ) pair potential:

$$\varphi(r) = 4\varepsilon \left[\left(\frac{\sigma}{r} \right)^{12} - \left(\frac{\sigma}{r} \right)^{6} \right]. \tag{4}$$

The basic parameters were $\sigma_{Ar-Ar} = 0.341$ nm, $\varepsilon_{Ar-Ar} = 1.67 \times 10^{-21}$ J, $\sigma_{C-Ar} = 0.357$ nm, and $\varepsilon_{C-Ar} = 1.97 \times 10^{-21}$ J[39,40]. The C-C interactions were not considered since the nanotube was assumed to be a rigid body[32], so a larger time step of 10 fs could be used in the calculations. The time-consuming calculations of the interparticle interactions were reduced by using a cutoff distance of 0.77 nm. The *NVT* canonical ensemble was used with the Nose-Hoover thermostat.

The superimposed simple linear shear flow was realized by utilizing the SLLOD algorithm[41]. The Lee-Edwards boundary condition[42] was applied in the y direction, which is the velocity gradient direction with periodic boundary conditions for the other two directions. The excess heat produced by the shear flow was extracted by the thermostat. The thermostat was only applied in two directions (y, z) and not in the flow direction (x)[43-45]. The results were collected after 3×10^5 time steps (3000 ps) to allow time for the flow to develop.

1. Reuel, N. F., Dupont, A., Thouvenin, O., Lamb, D. C. & Strano, M. S. Three-dimensional tracking of carbon nanotubes within living cells. *ACS Nano* **6**, 5420–5428 (2012).
2. Strano, M. S. & Jin, H. Where is it heading? Single-particle tracking of single-walled carbon nanotubes. *ACS Nano* **2**, 1749–1752 (2008).
3. Dupont, A. & Lamb, D. C. Nanoscale three-dimensional single particle tracking. *Nanoscale* **3**, 4532–4541 (2011).
4. Jin, S. & Verkman, A. S. Single particle tracking of complex diffusion in membranes: simulation and detection of barrier, raft, and interaction phenomena. *J. Phys. Chem. B* **111**, 3625–3632 (2007).
5. Tsyboulski, D. A., Bachilo, S. M., Kolomeisky, A. B. & Weisman, R. B. Translational and rotational dynamics of individual single-walled carbon nanotubes in aqueous suspension. *ACS Nano* **2**, 1770–1776 (2008).
6. Han, Y. *et al.* Brownian motion of an ellipsoid. *Science* **314**, 626–630 (2006).
7. Günther, A., Bender, P., Tschöpe, A. & Birringer, R. Rotational diffusion of magnetic nickel nanorods in colloidal dispersions. *J. Phys.: Condens. Matter* **23**, 325103–14 (2011).
8. Yoshinari, Y., Kalay, Z. & Harada, Y. Observing the rotational diffusion of nanodiamonds with arbitrary nitrogen vacancy center configurations. *Phys. Rev. B* **88**, 235206–8 (2013).
9. Dhar, P. *et al.* Autonomously moving nanorods at a viscous interface. *Nano Lett.* **6**, 66–72 (2006).
10. Xiao, L., Qiao, Y., He, Y. & Yeung, E. S. Imaging translational and rotational diffusion of single anisotropic nanoparticles with planar illumination microscopy. *J. Am. Chem. Soc.* **133**, 10638–10645 (2011).
11. Maragó, O. M. *et al.* Brownian motion of grapheme. *ACS Nano* **4**, 7515–7523 (2010).
12. Kang, P., Serey, X., Chen, Y.-F. & Erickson, D. Angular orientation of nanorods using nanophotonic tweezers. *Nano Lett.* **12**, 6400–6407 (2012).
13. Miller, R. D. & Jones, T. B. Electro-orientation of ellipsoidal erythrocytes. Theory and experiment. *Biophys. J.* **64**, 1588–1595 (1993).
14. Kim, J. H. *et al.* The rational design of nitric oxide selectivity in single-walled carbon nanotube near-infrared fluorescence sensors for biological detection. *Nat. Chem.* **1**, 473–481 (2009).
15. Liu, K. *et al.* Scratch-resistant, highly conductive, and high-strength carbon nanotube-based composite yarns. *ACS Nano* **4**, 5827–5834 (2010).
16. Falvo, M. R. *et al.* Bending and buckling of carbon nanotubes under large strain. *Nature* **389**, 582–584 (1997).
17. Al-Saleh, M. H. & Sundararaj, U. A review of vapor grown carbon nanofiber/polymer conductive composites. *Carbon* **47**, 2–22 (2009).
18. Jayalakshmi, V. & Prasad, S. K. Understanding the observation of large electrical conductivity in liquid crystal-carbon nanotube composites. *Appl. Phys. Lett.* **94**, 202106–3 (2009).
19. Zhang, D. H. *et al.* Transparent, conductive, and flexible carbon nanotube films and their application in organic light-emitting diodes. *Nano Lett.* **6**, 1880–1886 (2006).
20. Behabtu, N. *et al.* Strong, light, multifunctional fibers of carbon nanotubes with ultrahigh conductivity. *Science* **339**, 182–186 (2013).
21. Schoch, R. B., Han, J. & Renaud, P. Transport phenomena in nanofluidics. *Rev. Mod. Phys.* **80**, 839–883 (2008).
22. Zhang, J.-X. *et al.* Direct synthesis of solvent-free multiwall carbon nanotubes/silica nonionic nanofluid hybrid material. *ACS Nano* **3**, 2185–2190 (2009).
23. Lu, L. & Chen, W. Large-scale aligned carbon nanotubes from their purified, highly concentrated suspension. *ACS Nano* **4**, 1042–1048 (2010).
24. Zan, X., Feng, S., Balizan, E., Lin, Y. & Wang, Q. Facile method for large scale alignment of one dimensional nanoparticles and control over myoblast orientation and differentiation. *ACS Nano* **7**, 8385–8396 (2013).
25. Hobbie, E. K. Shear rheology of carbon nanotube suspensions. *Rheol. Acta.* **49**, 323–334 (2010).
26. Jeffery, G. B. Motion of ellipsoidal particles immersed in a viscous fluid. *Proc. R. Sot. Lond. A* **102**, 161–179 (1922).
27. Cox, R. G. The motion of long slender bodies in a viscous fluid. Part 2. Shear flow. *J. Fluid Mech.* **45**, 625–657 (1971).
28. Stover, C. A., Koch, D. L. & Cohen, C. Observations of fiber orientation in simple shear flow of semi-dilute suspensions. *J. Fluid Mech.* **238**, 277–296 (1992).
29. Fiahnama, M., Koch, D. L. & Shaqfeh, E. S. G. The effect of hydrodynamic interactions on the orientation distribution in a fiber suspension subject to simple shear flow. *Phys. Fluids* **7**, 487–506 (1995).
30. Leal, L. G. & Hinch, E. J. The effect of weak Brownian rotations on particles in shear flow. *J. Fluid Mech.* **46**, 685–703 (1971).
31. Hinch, E. J. & Leal, L. G. The effect of Brownian motion on the rheological properties of a suspension of non-spherical particles. *J. Fluid Mech.* **62**, 683–712 (1972).
32. Tang, W. & Advani, S. G. Nonequilibrium Molecular Dynamics Simulation to Describe the Rotation of Rigid, Low Aspect ratio Carbon Nanotubes in Simple Shear Flow. *J. Chem. Phys.* **126**, 144711–6 (2007).
33. Tannous, C. Langevin simulations of rod-shaped object alignment by surface flow. *Surf. Sci.* **605**, 923–929 (2011).
34. Skjetne, P., Ross, R. F. & Klingenberg, D. J. Simulation of single fiber dynamics. *J. Chem. Phys.* **107**, 2108–2121 (1997).
35. Cao, B. Y. & Dong, R. Y. Molecular dynamics calculation of rotational diffusion coefficient of a carbon nanotube in fluid. *J. Chem. Phys.* **140**, 034703–5 (2014).
36. Kumar, A. & Higdon, J. J. L. Dynamics of the orientation behavior and its connection with rheology in sheared non-Brownian suspensions of anisotropic dicolloidal particles. *J. Rheol.* **55**, 581–626 (2011).
37. Börzsönyi, T. *et al.* Orientational order and alignment of elongated particles induced by shear. *Phys. Rev. Lett.* **108**, 228302–5 (2012).
38. Plimpton, S. Fast parallel algorithms for short-range molecular dynamics. *J. Comp. Phys.* **117**, 1–19 (1995).
39. Cao, B. Y. & Hou, Q. W. Thermal conductivity of carbon nanotubes embedded in solids. *Chin. Phys. Lett.* **25**, 1392 (2008).
40. Tuzun, R. E., Noid, D. W., Sumpter, B. G. & Merkle, R. C. Dynamics of fluid flow inside carbon nanotubes. *Nanotechnology* **7**, 241 (1996).
41. Evans, D. J. & Morriss, G. P. *Statistical Mechanics of Nonequilibrium Liquids* (Academic, London, 1990).
42. Lee, A. W. & Edwards, S. F. The computer study of transport processes under extreme conditions. *J. Phys. C: Solid State Phys.* **5**, 1921–1929 (1972).
43. Grest, G. S. & Kremer, K. Molecular dynamics simulation for polymers in the presence of a heat bath. *Phys. Rev. A* **33**, 3628 (1986).
44. Cao, B. Y., Chen, M. & Guo, Z. Y. Temperature dependence of the tangential momentum accommodation coefficient for gases. *Appl. Phys. Lett.* **86**, 091905 (2005).
45. Cao, B. Y., Chen, M. & Guo, Z. Y. Liquid flow in surface-nanostructured channels studied by molecular dynamics simulation. *Phys. Rev. E* **74**, 066311 (2006).

Acknowledgments

Author contributions

R.Y.D. designed the project, performed the calculations and wrote the paper. B.Y.C. discussed the results, revised and commented on the manuscript.

Additional information